THE JOURNAL OF BIOLOGICAL CHEMISTRY
Vol. 275, No. 12, Issue of March 24, pp. 9011–9018, 2000

Printed in U.S.A.

Characterization of the N-terminal Domain of the Yeast Transcriptional Repressor Tup1

PROPOSAL FOR AN ASSOCIATION MODEL OF THE REPRESSOR COMPLEX Tup1·Ssn6*

(Received for publication, July 22, 1999, and in revised form, December 21, 1999)

Carole Jabet‡§, Elizabeth R. Sprague‡, Andrew P. VanDemark‡, and Cynthia Wolberger‡§¶

From the ‡Department of Biophysics and Biophysical Chemistry and the §Howard Hughes Medical Institute, Johns Hopkins University School of Medicine, Baltimore, Maryland 21205

The yeast Tup1 and Ssn6 proteins form a transcriptional repression complex that represses transcription of a broad array of genes. It has been shown that the N-terminal domain of the Tup1 protein interacts with a region of the Ssn6 protein that consists of 10 tandem copies of a tetratricopeptide motif. In this work, we use a surface plasmon resonance assay to measure the affinity of the N-terminal domain of Tup1 for a minimal 3-TPR domain of *Saccharomyces cerevisiae* Ssn6 that is sufficient for binding to Tup1. This domain of Ssn6 binds with comparable affinity to *S. cerevisiae* and *Candida albicans* Tup1, but with 100-fold lower affinity to Tup1 protein containing a point mutation that gives rise to a defect in repression *in vivo*. Results from studies using analytical ultracentrifugation, CD spectroscopy, limited proteolysis, and ^{1}H NMR show that this domain of Tup1 is primarily α-helical and forms a stable tetramer that is highly nonglobular in shape. X-ray diffraction recorded from poorly ordered crystals of the Tup1 tetramerization domain contains fiber diffraction typical of a coiled coil. Our results are used to propose a model for the structure of the N-terminal domain of Tup1 and its interaction with the Ssn6 protein.

Transcriptional repression of a variety of yeast genes is mediated by two proteins that act in concert, Ssn6 and Tup1. These proteins are required for the repression of at least five independently regulated sets of genes: the mating type **a**- and haploid-specific genes (1, 2), glucose-repressed genes (3, 4), hypoxic genes (5), and DNA damage-inducible genes (6). Tup1 and Ssn6 have been shown to form a corepressor complex that is recruited to the DNA by interaction with sequence-specific DNA-binding proteins such as Matα2, Rox1, Mig1, and the Crt repressor (2, 7–11). The Tup1·Ssn6 corepressor complex has been estimated by sucrose gradient sedimentation and by gel densitometry to contain three or four Tup1 subunits and one Ssn6 subunit (12, 13). Although mutations in either protein give rise to defects in transcriptional repression (1, 3, 14–18), Tup1 appears to play the predominant role, because the defect in repression that results from deletion of both the Ssn6 and Tup1 genes can be overcome by overexpression of Tup1, but not Ssn6 (19). Moreover, Ssn6-LexA fusions repress transcription in a Tup1-dependent manner, whereas Tup1-LexA fusions can repress transcription in the absence of Ssn6 (20). The mechanism of repression by Tup1·Ssn6 is not well understood, although there is evidence that it occurs by either direct interaction with the polymerase II holoenzyme (21, 22) or by altering local chromatin structure (23, 24).

The functional domains of the 713-amino acid Tup1 protein from the yeast *Saccharomyces cerevisiae* have been analyzed by genetic and biochemical approaches. The N-terminal residues 1–72 contain sequences that are involved in complex formation with Ssn6 (20) as well as mediating multimerization of Tup1 (12, 20). Residues 120–334 contain sequences that mediate transcriptional repression, as determined by the inability of Tup1 fragments lacking this region to repress transcription (20). The C-terminal half of Tup1 (residues 334–713) consists of a domain that contains seven WD40 repeats. These repeats, also known as β-transducin motifs (1, 25, 26), are present in many proteins that are involved in diverse cellular processes and have been suggested to mediate protein-protein interactions. In the case of Tup1, the WD motif has been shown to interact with the mating-type regulator, Matα2 (19, 27). Both the sequence and the biological function of Tup1 are conserved in the yeast *Candida albicans* whose 515-residue Tup1 protein is 48% identical to the *S. cerevisiae* Tup1 protein. Moreover, expression of the *C. albicans* Tup1 gene fully complements a *tup1* deletion in *S. cerevisiae* (28).

Ssn6 is a 966-amino acid protein that contains at its N terminus a domain of 10 tetratricopeptide repeats (TPR)[1] (residues 46–398) that is essential for its function (3, 14). The TPR is a motif of 34 amino acids found in over 30 proteins from a variety of organisms that have diverse cellular functions (for review see Ref. 29). Distinct combinations of TPR motifs are required for direct interaction with Tup1 and for repression of distinct classes of genes (11). For example, the first three TPR motifs are sufficient for binding to Tup1 (11) and to Matα2 (30) and for repression of mating-type regulated genes (11). Repeats 1–7 are necessary for the repression of oxygen-regulated genes, whereas all the TPR motifs are required for repression of DNA damage-regulated genes (11). As seen in the crystal structure of the 3-TPR domain of the protein phosphatase 5 (PP5) (31), a single TPR folds to form a pair of antiparallel α-helices of equal length. Successive TPRs pack against one another in tandem and are related by a small rotation. The uniform angular and spatial arrangement of neighboring α-helices generates a right-handed superhelix with a central groove (31).

In the present study, we use a surface plasmon resonance-based assay to quantitate the interaction between the N-terminal tetramerization domain of Tup1 and the minimal 3-TPR domain of *S. cerevisiae* Ssn6 that is sufficient for mediating

* This work was supported by the National Science Foundation Grant MCB 98-08412 and by the Howard Hughes Medical Institute. The costs of publication of this article were defrayed in part by the payment of page charges. This article must therefore be hereby marked "*advertisement*" in accordance with 18 U.S.C. Section 1734 solely to indicate this fact.

¶ To whom correspondence should be addressed. Tel.: 410-955-0728; Fax: 410-955-0637; E-mail: cwolberg@jhmi.edu.

[1] The abbreviations used are: TPR, tetratricopeptide repeats; PP5, protein phosphatase 5.

interactions with Tup1 (20). We show that the affinity for Ssn6 of both the *S. cerevisiae* and *C. albicans* Tup1 is comparable, whereas the *S. cerevisiae* Tup1 containing an L62R substitution binds 100-fold more weakly to Ssn6. Equilibrium ultracentrifugation of the wild type and mutant proteins shows that this mutation, which has a deleterious effect on Tup1-mediated repression *in vivo*, does not interfere with the tetramerization of Tup1 and is therefore likely to lie on the surface of the Tup1 tetramer. Using a combination of analytical ultracentrifugation, circular dichroism (CD) spectroscopy, proteolysis, ^{1}H NMR, and x-ray fiber diffraction, we characterize structural features of the tetramerization domain. We find that this domain is highly nonglobular in shape and associates to form a type of α-helical coiled coil. These results are used to propose a model for the structure of the N-terminal domain of Tup1 and its interaction with the TPR domain of Ssn6.

EXPERIMENTAL PROCEDURES

Mutagenesis—The modification of the cDNA encoding the N-terminal domain of Tup1 carrying the mutation Leu-62 → Arg (Sc mut62 Tup1) was obtained with the QuickChange™ mutagenesis kit (Stratagene) following the instructions of the manufacturer.

Protein Expression and Purification—The cDNAs encoding the respective N-terminal domains of *S. cerevisiae* Tup1 (Sc N91 Tup1; residues 1–91) and of *C. albicans* Tup1 (Ca N92 Tup1; residues 1–92) as well as the N-terminal domain of Tup1 carrying the mutation Leu-62 → Arg (Sc mut62 Tup1) were cloned in the pET 3d vector (Novagen). Each fragment is preceded by an additional methionine and is expressed in *Escherichia coli* under control of the T7 promoter. BL21 (DE3) pLysS cells were grown at 37 °C in LB medium with 100 μg/ml ampicillin, induced at mid-log phase with 1 mM isopropyl-1-thio-β-D-galactopyranoside, and grown for 3 h at 25 °C. The bacterial cell pellet was sonicated in 1× phosphate-buffered saline, 0.8 M NaCl, 10% glycerol, 1% Igepal, and 1 mM EDTA. The lysate was centrifuged at 8500 rpm in a GSA rotor for 15 min. The protein was precipitated with 20% ammonium sulfate and resuspended in 50 mM Tris (pH 8), 50 mM NaCl, and 1 mM EDTA. Ion exchange chromatography was performed on the protein solution with a Q Fast Flow column (Amersham Pharmacia Biotech) followed by a MonoQ column (Amersham Pharmacia Biotech). In each case, protein solutions were loaded onto columns equilibrated in 50 mM Tris (pH 8), 50 mM NaCl, and 1 mM EDTA and eluted with a 0.05–1 M NaCl gradient. Peak fractions were pooled and purified by gel filtration using a Superdex 75 column (Amersham Pharmacia Biotech) in 50 mM Tris (pH 8), 150 mM NaCl, and 1 mM EDTA. Proteins were then dialyzed against 10 mM Tris (pH 8) and 25 mM NaCl, concentrated to 10 mg/ml, and stored at −80 °C.

The cDNA encoding the first three TPR motifs of *S. cerevisiae* Ssn6 (residues 31–149) was cloned in the pET 16b vector (Novagen), which directs protein expression in *E. coli* under control of the T7 promoter. The Ssn6 fragment is preceded by a 10 histidine tag and the sequence SSGHIQGAH, which contains a factor Xa cleavage site. BL21 (DE3) pLysS cells were grown at 37 °C in LB medium with 100 μg/ml ampicillin, induced at mid-log phase with 1 mM isopropyl-1-thio-β-D-galactopyranoside, and grown for 3 h at 25 °C. The bacterial cell pellet was sonicated in 1× phosphate-buffered saline, 0.8 M NaCl, 10% glycerol, 1% Igepal, 1 mM EDTA, and 2 M urea. The lysate was centrifuged in a GSA rotor at 8500 rpm for 15 min, after which the protein was found in the insoluble fraction. This fraction was resuspended in 20 mM Tris (pH 8), 500 mM NaCl, and 6M urea, filtered, and loaded onto a HisTrap column (Amersham Pharmacia Biotech) equilibrated in 20 mM Tris (pH 8), 500 mM NaCl, and 6 M urea. The elution was performed with a 0–1 M imidazole gradient. Peak fractions were pooled, diluted to 10 μg/ml, and dialyzed against 50 mM Tris (pH 8) and 50 mM NaCl.

Analytical Ultracentrifugation—Sedimentation equilibrium experiments were conducted using a Beckman Optima XL-A analytical ultracentrifuge equipped with an optical absorbance system. Runs were carried out at 9000, 10,000, 13,000, 15,000, 20,000, and 27,000 rpm at 20 °C. Six-channel, charcoal-filled epon centerpieces with quartz windows were used in an An-60 Ti rotor. Samples at concentrations of 1.7, 0.8, and 0.4 mg/ml, in 50 mM Tris (pH 8) and 150 mM NaCl were analyzed. Cells were loaded with 100 μl of protein sample and 110 μl of reference buffer. Radial scans at 280 nm were collected between 5.9 and 7.2 cm as the average of five measurements, with a step size of 0.001 cm. The samples were allowed to achieve sedimentation equilibrium over the course of 26 h and were judged to be at equilibrium when sequential scans 2 h apart were superimposable. The proteins' partial specific volumes (Sc N91 Tup1, 0.726 g/ml and Sc mut62 Tup1, 0.7241 g/ml), buffer density (1.0058 g/ml), buffer viscosity (1.0312×10^{-2} poise), and temperature corrections were determined using standard methods (for review of methods, see Ref. 32), as implemented in the SEDNTERP program. Sedimentation equilibrium data were analyzed using the appropriate functions by nonlinear least squares procedures (33) provided in the Beckman Optima XL-A software package.

For data analysis according to discrete self-association models, the following general equation was used,

$$C(r) = \delta + C_{1.0}\exp(\sigma(r^2 - r_0^2)) + \sum_{N>1} C_{1.0}^N K_N \exp(N\sigma(r^2 - r_0^2)) \quad \text{(Eq. 1)}$$

where $C(r)$ is the total concentration at radius r, δ is the base-line offset, $C_{1,0}$ is the monomer concentration at the reference radius r_o, N is the stoichiometry of the reaction, and K_N is the equilibrium association constant. σ is defined as follows,

$$\sigma = M_1(1 - \bar{\nu}\rho)\omega^2/2RT \quad \text{(Eq. 2)}$$

where M_1 is the monomer molecular weight, $\bar{\nu}$ is the partial specific volume, ρ is the solvent density, ω is the angular velocity of the rotor, R is the gas constant, and T is the absolute temperature of the sedimentation equilibrium experiment. Global molecular weights were obtained for several rotor speeds and protein concentrations by fitting the equilibrium sedimentation data to a single species using the equations above.

Sedimentation velocity experiments were carried out at 60,000 rpm at 20 °C for sample concentrations of 0.18, 1.1, and 1.3 mg/ml. Protein and buffer samples were prepared as described above. Two-sector charcoal-filled epon 12-mm centerpieces with quartz windows were loaded with 420 μl of protein in the sample well and 426 μl of buffer in the reference well. Radial scans at 230 or 280 nm were collected with a step size of 0.003 cm in continuous mode at intervals of about 4 min for a period of 4 h. Sedimentation coefficients corrected for diffusion were calculated for each boundary by the method of van Holde and Weischet (34) using the program Ultrascan II (B. Demeler, University of Texas Health Sciences Center at San Antonio). The $s_{20,w}$ for each protein concentration was determined at the boundary midpoint from a plot of the boundary fraction *versus* $S_{20,w}$. Values of $s_{20,w}$ at three different protein concentrations did not show evidence of concentration dependence when extrapolated to infinite dilution. Thus, the $s^0_{20,w}$ of 2.24 ± 0.01 S was obtained by averaging the three sedimentation coefficients. The translational frictional coefficient, f, was calculated from the Svedberg equation,

$$f = \frac{M(1 - \bar{\nu}\rho)}{N_A s} \quad \text{(Eq. 3)}$$

where $\bar{\nu}$ is the partial specific volume, ρ is the solvent density, M is the molecular weight, N_A is Avogadro's number, and s is the sedimentation coefficient. The frictional coefficient for a rigid spherical molecule of equal (anhydrous) volume, f_o, was calculated from Stokes law, $f_o = 6\pi\eta R_o$ where η is the buffer viscosity and R_o is the radius of the molecule. Based on the frictional coefficient and an estimated value for hydration from the amino acid composition ($\delta = 0.4244$) (32), axial ratios for simple ellipsoidal and cylindrical models were estimated using SEDNTERP.

Surface Plasmon Resonance Experiments—Assays of the Tup1-Ssn6 interaction were performed on a Biacore system with certified nitrilotriacetic acid sensor chips. Flow cells were coated with nickel as described by the manufacturer. Immobilization of the His-3TPR Ssn6 and of the His-AraC (control) fragments was performed as follows. A continuous flow of running buffer (50 mM Tris (pH 8) and 150 mM NaCl) over the sensor surface at 10 μl/min was maintained and between 60 and 150 μl of HisTag fragments (200 nM in 50 mM Tris (pH 8) and 50 mM NaCl) were injected at 3 μl/min. The relative amount of protein immobilized ranged from 250 to 400 response units. Binding of the N-terminal Tup1 fragments to the immobilized Ssn6 3 TPR protein was monitored by injecting 20 μl of Tup1 at increasing concentrations (2–20 μM) over the chip surface at a flow rate of 10 μl/min at 25 °C. After 15 min of dissociation, the surface was regenerated.

Kinetic Analysis of Plasmon Resonance Results—Interaction curves were obtained by subtracting the experimental curves from the control. Data were analyzed using the Langmuir model functions provided in the Biacore Biaevaluation 3.0 software package. According to this model, data were evaluated using the following rate equation,

$$dR/dt = k_a C(R_{max} - R_t) - k_d R_t \quad \text{(Eq. 4)}$$

assuming a single site interaction between the Ssn6 3 TPR protein and each N-terminal Tup1 tetramer, where dR/dt is the rate of formation of surface complexes, C is the concentration of N-terminal Tup1 tetramer, R_{max} is the total amount of immobilized ligand expressed as surface plasmon resonance response, R_t is the response observed at time t. k_a and k_d are the association and dissociation rate constants, respectively. The equilibrium dissociation constant, K_D, was calculated from the ratio k_d/k_a. The fit of the data to the model was assessed by examining the residuals and by minimizing the χ^2 values.

Measurement of CD Spectra—CD spectra of the N-terminal Tup1 fragments were measured at 20 °C in a AVIV DS 60 spectrometer with a quartz cell of 0.1-mm path length. The protein concentration was 1 mg/ml in 10 mM phosphate buffer (pH 7). Molar ellipticity was calculated as described by Delage and Geourjon (35). Estimates of the secondary structure were made using the CDNN program (36, 37).

NMR Data Collection—The Sc N91 Tup1 fragment was concentrated to 1 mM in 20 mM phosphate buffer (pH 7). The ^{1}H nuclear Overhauser effect spectroscopy spectrum was collected with Brucker DMX 600 MHz at 25 °C in 90% H_2O − 10% D_2O. The spectrum was processed with NMRPipe (38).

Crystallization and X-ray Diffraction—Crystals of the N-terminal domain of Tup1 were grown by the method of hanging drop vapor diffusion from protein purified and concentrated as described above. Protein was mixed on a siliconized coverslip with an equal volume of well solution containing 12% (w/v) polyethylene glycol 4000, 100 mM Bis-Tris propane (pH 9), and 1 mM dithiothreitol and suspended over the well solution, after which crystals appeared in 1–2 weeks. Crystals of dimension 600 × 400 × 50 μm were mounted and sealed in a glass capillary. X-ray diffraction was recorded at room temperature with an RAXIS II image plate detector equipped with Osmic double-focusing mirrors using copper Kα radiation generated by a Rigaku RU-200 rotating anode x-ray generator. Unit cell and fiber diffraction parameters were measured directly from diffraction images using the program IPDISP (54).

RESULTS

The N-terminal Domain of Tup1 Mediates Tetramerization That Is Not Impaired by the Mutation L62R—Comparison of several fungal Tup1 proteins reveals the presence of a conserved 10-kDa N-terminal domain containing residues that have been found to mediate tetramerization of *S. cerevisiae* Tup1 (12, 20) and interaction with Ssn6 (20). The corresponding domain of *S. cerevisiae* Tup1 containing residues 1–91 (Sc N91 Tup1) was expressed and purified, and its oligomeric state was assayed by sedimentation equilibrium analytical ultracentrifugation. Typical data collected at one initial loading concentration and at three different speeds are shown in Fig. 1*A*. These data, as well as additional data collected at different initial loading concentrations (data not shown), were well described by a model for a single homogeneous species ("Experimental Procedures," Equation 1) as evaluated by randomness of the residuals and minimization of the variance (Fig. 1*A*). The single species model yielded an average molecular mass of 43,000 Da ± 1500, which compared with the calculated monomer molecular mass of 11,088 Da, strongly suggests that Sc N91 Tup1 self-associates as a tetramer. To examine whether monomer, dimer, or octamer species were also present, the data were also fit to models describing monomer-dimer-tetramer, monomer-tetramer, and monomer-tetramer-octamer equilibria. Attempts to fit the data to each of these models were unsuccessful as reflected in increased variances as well as unrealistic values for equilibrium constants. We therefore conclude that the tetramer is the predominant species of Sc N91 Tup1 and that this tetramer is not in a detectable reversible equilibrium with other species.

Carrico and Zitomer (39) identified a Tup1 mutant protein with leucine 62 replaced by an arginine, L62R, which is unable to form a complex with Ssn6 or to repress expression of hypoxic and glucose-repressed reporter genes. Repression of the **a**-mating type reporter gene, however, is unaffected by this substitution. To better understand the effects of this mutation, we used equilibrium analytical ultracentrifugation to examine whether the mutation Leu-62 → Arg impairs the ability of Sc N91 Tup1 to form a tetramer. Data collected for one loading concentration of Sc mut62 Tup1 at three different speeds are shown in Fig. 1*B*. These data with additional data at two other loading concentrations (data not shown) fit best to a model with a single species of molecular mass 40,000 ± 1000 Da. Because the calculated monomer molecular mass of Sc mut62 Tup1 is 11,131 Da, the predominant oligomeric state of Sc mut62 Tup1 is a tetramer, as was observed for the wild-type fragment. In

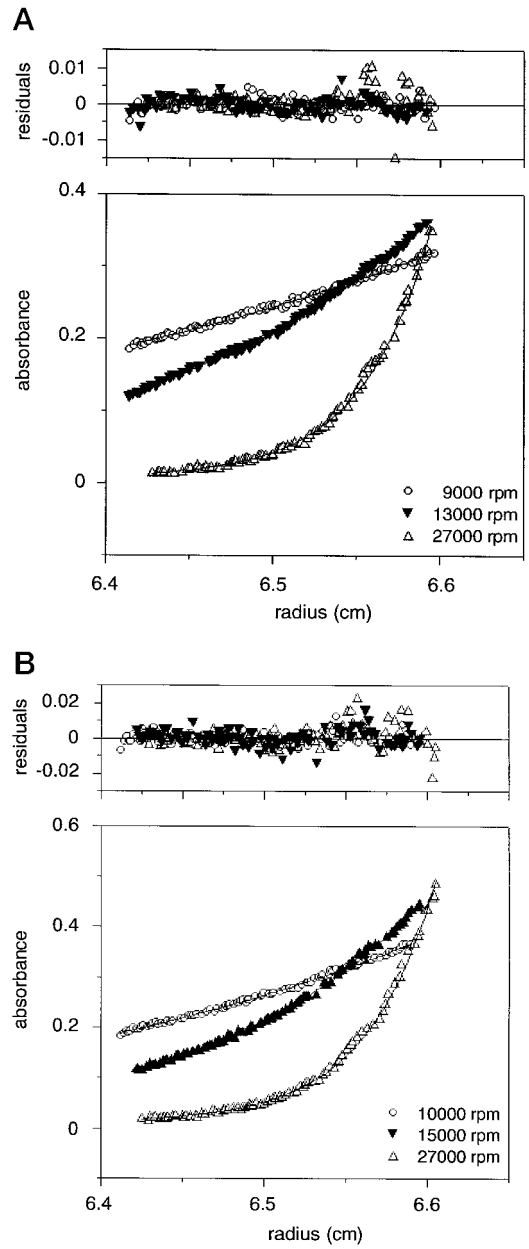

FIG. 1. *A*, sedimentation equilibrium analytical ultracentrifugation of Sc N91 Tup1. The absorbance *versus* radius profile for 52 μM Sc N91 Tup1 at 9000, 13,000, and 27,000 rpm at 20 °C is shown in the *lower panel*. *Circles* and *triangles* are the data points, and the solid line is the model as described by Equation 1 ("Experimental Procedures"). The residuals of the fit to Equation 1 are shown in the *upper panel*. *B*, sedimentation equilibrium analytical ultracentrifugation of Sc mut62 Tup1. The absorbance *versus* radius profile for 58 μM Sc mut62 Tup1 at 10,000, 15,000, and 27,000 rpm at 20 °C is shown in the *lower panel*. *Circles* and *triangles* are the data points, and the *solid line* is the model as described by Equation 1 ("Experimental Procedures"). The residuals of the fit to Equation 1 are shown in the *upper panel*.

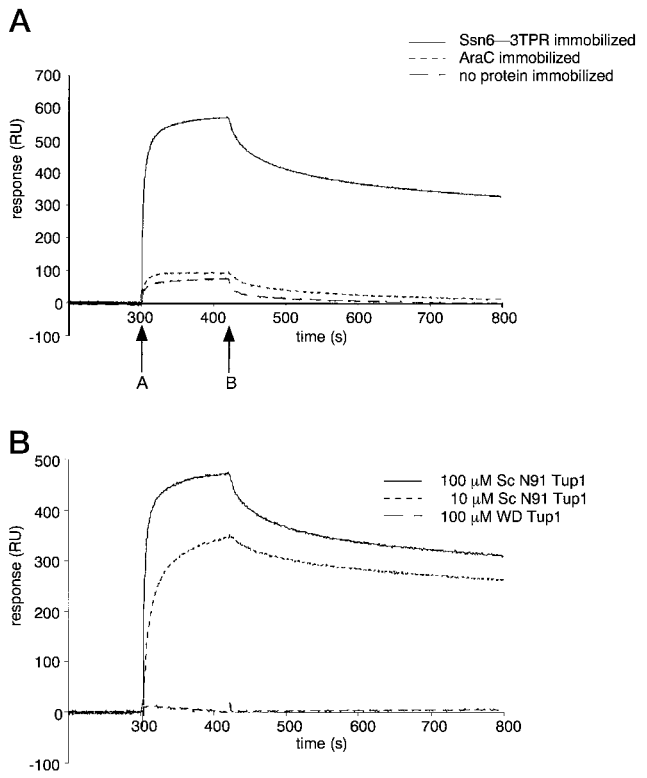

FIG. 2. **Surface plasmon resonance assay of the N-terminal domain of Tup1 binding to the first three TPR motifs of Ssn6.** *A,* sensorgrams showing injection of 100 μM Sc N91 Tup1 over surfaces coupled with the 3 TPR-Ssn6 protein, the AraC protein, or a noncoupled surface (Ni^{+}-coated surface). Injection started at time *A* and ended at time *B*. Changes in the signal observed with the AraC-coupled or the noncoupled surfaces were because of the Sc N91 Tup1 protein affecting the bulk refractive index of the running buffer. These changes are also observed at the start and the end of the injection with the 3 TPR-Ssn6-coupled surface and are subtracted as background to give the net sensorgrams. *B,* net sensorgrams showing injection of Sc N91 Tup1 (100 and 10 μM) and of Sc WD Tup1 (100 μM). *RU*, response units.

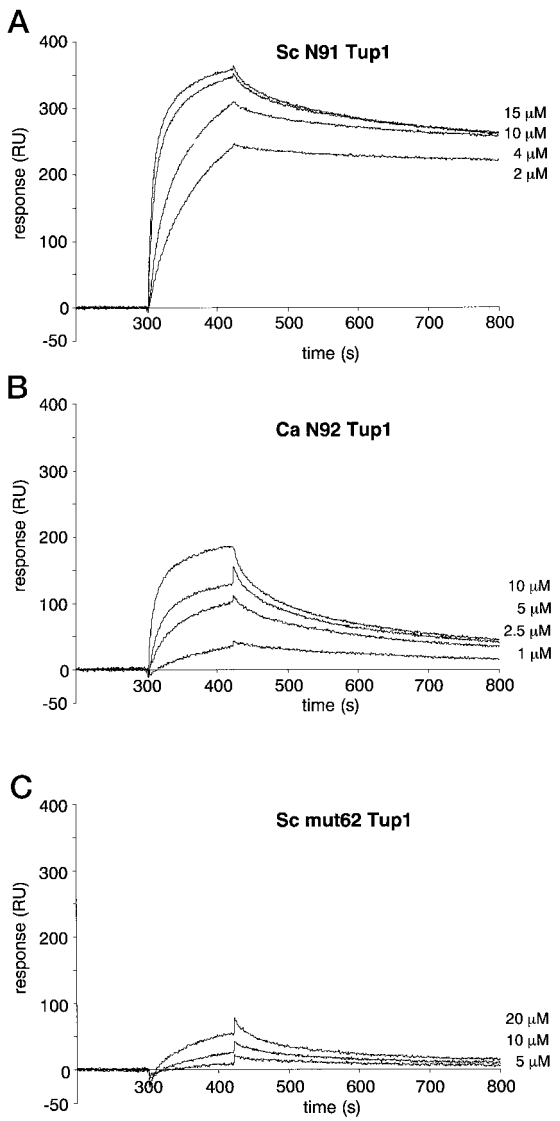

FIG. 3. **Surface plasmon resonance kinetic analysis of the N-terminal domain of Tup1 interaction with the first three TPR motifs of Ssn6.** Representative net sensorgrams illustrating the real-time binding of various concentrations of Sc N91 Tup1 (*a*), Ca N92 Tup1 (*b*), and Sc mut62 Tup1 (*c*) to the 3TPR-Ssn6 fragment immobilized on the sensor chip. Analyses were performed as described under "Experimental Procedures," and the results are summarized in Table I. *RU*, response units.

light of the 4500 Da difference between the observed molecular mass and the theoretical one, it is possible that some monomer or dimer states are also present in solution. However, attempts to fit the data to monomer-dimer-tetramer, monomer-tetramer, or dimer-tetramer models were unsuccessful, as shown again by increased variances and unrealistic values for equilibrium constants. These results show that the tetramerization of the N-terminal domain of Tup1 is very stable and is not in a reversible equilibrium with lower oligomeric states. They also demonstrate that the mutation L62R, which weakens the interaction with Ssn6, does not notably impair the tetramerization of Tup1.

Affinity of the Ssn6/Tup1 Interaction—A surface plasmon resonance-based biosensor assay was used to carry out a kinetic analysis of the Tup1-Ssn6 interaction. The protein fragments assayed were those that had been previously shown to be the minimal domains required for the two proteins to bind to one another (11, 20). An Ssn6 fragment consisting of the first three TPR motifs (residues 31–149) and preceded by an N-terminal His tag was immobilized on a Ni^{2+}-coated biosensor chip surface (see "Experimental Procedures"). The binding of the Tup1 protein to the surface of the chip and its subsequent dissociation were monitored by surface plasmon resonance, which yields a signal proportional to the mass detected. The sensorgram in Fig. 2*A* shows the binding of the Sc N91 Tup1 fragment to the immobilized Ssn6 3 TPR fragment. As a control for the specificity of the interaction, this was compared with the binding of Tup1 to a surface coupled with the N-terminal domain of the *E. coli* AraC protein fused to a His tag (Fig. 2*A*) and to a Ni^{2+}-coated surface lacking immobilized protein (Fig. 2*A*). Binding of Tup1 to either surface was negligible. Furthermore, a Tup1 fragment containing the WD region of the protein but lacking the N-terminal residues that interact with Ssn6 (Sc WD Tup1), did not bind to the immobilized Ssn6 3TPR fragment, even at high concentrations (Fig. 2*B*).

Binding of Sc N91 Tup1 to the immobilized Ssn6 3 TPR fragment was studied over a Sc N91 Tup1 concentration range of 2–15 μM. Fig. 3*A* shows representative sensorgrams of association and dissociation at various Sc N91 Tup1 concentrations. These data were analyzed by simultaneous global fitting of both association and dissociation phases for all sets of concentrations, using the model AB 219 A+B and assuming a single site interaction between a Tup1 tetramer and Ssn6 ("Experimental Procedures," Equation 1). The best fit was achieved by considering the first three minutes of the dissociation (χ^2 = 17.5, Table I). According to this fit, the dissociation rate, k_d, was equal to 8×10^{-4} s^{-1}, and the association rate, k_a, was

TABLE I
Kinetic and equilibrium constants for the interaction of Tup1 with the first three TRR motifs of Ssn6, as determined by surface plasmon resonance

	k_a	k_d	K_D	χ^2
	$M^{-1}\ s^{-1}$	s^{-1}	M	
Sc N91 Tup1	6.4×10^3	8×10^{-4}	1.2×10^{-7}	17.5
Ca N92 Tup1	4.8×10^3	2.2×10^{-3}	4.5×10^{-7}	28
Sc mut62 Tup1	4.8×10^2	5.1×10^{-3}	1×10^{-5}	2.4

equal to 6.4×10^3 M^{-1} s^{-1}, yielding a value for the equilibrium dissociation constant, K_D, of 1.2×10^{-7} M (Table I). Similar rate constants were found for the interaction between the Ssn6 3 TPR fragment and the Ca N92 Tup1 fragment (residues 1–92 of *C. albicans* Tup1) (Fig. 3*B* and Table I), which has an equilibrium dissociation constant K_D of 4.5×10^{-7} M.

We next evaluated the affinity of the Sc mut 62 Tup1 fragment for the Ssn6 3 TPR fragment. When the Sc mut62 Tup1 protein is injected on the surface with the immobilized Ssn6 3 TPR fragment (Fig. 3*C*), k_d and k_a were 5.1×10^{-3} s^{-1} and 4.8×10^2 M^{-1} s^{-1} respectively, leading to a calculated K_D of 1×10^{-5} M (Table I). The mutant Tup1 protein therefore binds to the Ssn6 3 TPR protein with a 100-fold lower affinity as compared with the wild-type fragment, Sc N91 Tup1.

The N-terminal Residues of Tup1 Form a Compact α-Helical Domain—CD spectroscopy was used to analyze the secondary structure of the N-terminal Tup1 fragments Sc N91 Tup1, Ca N92 Tup1, and Sc mut62 Tup1. The far UV CD spectrum of each fragment is similar (Fig. 4), with minima at 208 and 220 nm that are characteristic of a mainly helical protein. Based on these spectra, the proportions of secondary structural elements were estimated by the CDNN program (36, 37) to be 91.5% α-helix, 1.2% β-sheet, and 7.3% coil for Sc N91 Tup1, 94.6% α-helix, 0.8% β-sheet, and 4.6% coil for Ca N92 Tup1, and 85.2% α-helix, 1.9% β-sheet and 12.9% coil for Sc mut62 Tup1. These results show that the N-terminal domain of both *S. cerevisiae* and *C. albicans* Tup1 is highly α-helical in solution and that the mutation L62R in the *S. cerevisiae* Tup1 protein has only a minor effect on the overall secondary structural content.

The Sc N91 Tup1 fragment was subjected to limited proteolysis to assess whether it forms a compact structural domain (Fig. 5). The proteolysis was performed with subtilisin, which has a low specificity for substrate amino acids. The shortest resulting fragment (Fig. 5, *lanes 4*, *5*, and *6*) has a molecular mass of 10,609 Da determined by mass spectroscopy, whereas the molecular mass of undigested Sc N91 Tup1 determined by the same technique is 11,109 Da. N-terminal sequencing analysis of the proteolytic fragment showed that its first four residues were VSNT. These results are consistent with the removal of the first five residues of Sc N91 Tup1, MMTAS, which have a combined theoretical molecular mass of 540 Da. Taken together, these results indicate that the fragment that extends from residue 5 to 91 of Sc Tup1 forms a single structural unit.

The N-terminal Domain of Tup1 Is Nonglobular—To obtain further information on the tertiary structure of the N-terminal domain of Tup1, we collected a ^{1}H nuclear Overhauser effect spectroscopy NMR spectrum of the Sc N91 Tup1 fragment in solution. The spectrum shows that signals corresponding to exchanging amide protons are tightly grouped between 6.5 and 8 ppm (Fig. 6). There are no detectable methyl signals upfield of 0.5 ppm or amide signals downfield of 8.5 ppm, which would be typical of a globular protein. In folded, globular proteins, dispersion of amide and methyl group proton chemical shifts typically arises because of the differing local environment of various portions of the polypeptide chain. This variation is the result of the complete or partial burial of some residues in the protein's interior. The absence of dispersion in the case of the

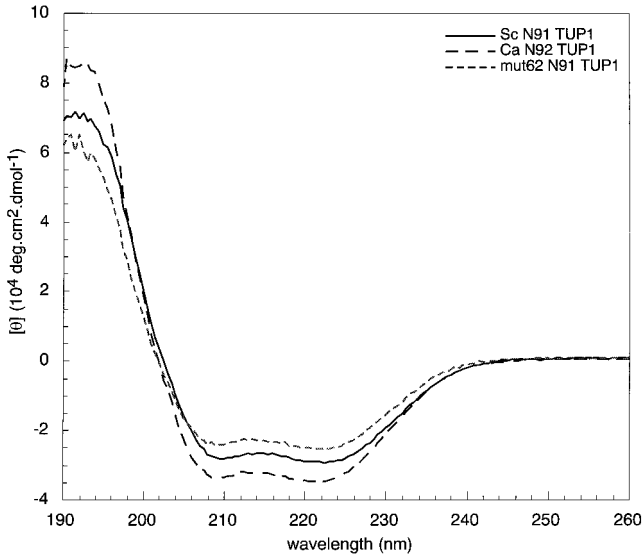

FIG. 4. **Circular dichroic spectra of the N-terminal domain of Tup1.** Spectra of wild type and mutant N-terminal domains of Tup1 measured in 10 mM phosphate buffer (pH 7) are shown.

Sc N91 Tup1 fragment indicates that the protein is likely nonglobular.

Sedimentation velocity analytical ultracentrifugation experiments were carried out to obtain further information regarding the overall shape of the Tup1 tetramerization domain. As shown in Fig. 7, the sedimentation coefficient is uniform across the entire boundary. The sedimentation coefficient corrected to standard conditions at infinite dilution, $s^0_{20,w}$, is 2.24 ± 0.01 S. The data are consistent with the sedimentation equilibrium studies that indicate a single species. The sedimentation coefficient is substantially lower than the value of 4.7 S expected for a globular protein with the molecular weight of the N91 Tup1 tetramer. The observed sedimentation coefficient of 2.24 S leads to a calculated value for the frictional ratio, f/f_o, of 2.09 for the Tup1 tetramer. The significant deviation of the frictional ratio of Sc N91 Tup1 from that expected for a globular protein (≈1.2 (40)) indicates that the Tup1 tetramerization domain is likely highly asymmetric or swollen because of unusual hydration. Based on the observed frictional ratio of 2.09 and a calculated hydration value (δ = 0.4224, see "Experimental Procedures"), three models for the overall shape of the tetramer give axial ratios of about 15 for a prolate ellipsoid, 20 for an oblate ellipsoid, and 16 for a cylinder.

Fiber Diffraction from Disordered Crystals of N91 Tup1 Indicate the Presence of a Coiled Coil—The x-ray diffraction pattern recorded from crystals of N91 Tup1 exhibits substantial crystal lattice disorder. The crystals form with an apparent orthogonal unit cell of a = 30 Å, b = 30 Å, and c = 266 Å, although there were insufficient data to make a definitive unit cell determination or assign the space group. As shown in Fig. 8, lattice reflections are visible in the central region to d spacings of 8 Å, with additional streaks and intense spots in the 4.7–5.0 Å region lying along the vertical direction. Strong diffuse diffraction is also observed at 10 Å resolution along the

horizontal axis. These features are characteristic of fiber diffraction from coiled coils oriented along the vertical C axis (41, 42). The equatorial 10 Å spacing results from the average side-by-side spacing of α-helices in the coiled coil, whereas the meridional streaks in the 4.9 Å region correspond to the rise/turn in each helix of the coiled coil. The precise value of the rise, which is 5.1 Å in the classic model of the coiled coil proposed by Crick (42), is a function of the helix-crossing angle in the coiled coil. A straight α-helix has a rise/turn of 5.4 Å, with increasing values of helix-crossing angles within the coiled-coil superhelix resulting in lower values of rise.

DISCUSSION

We have demonstrated in this study that the N-terminal domain of Tup1 is highly α-helical in nature and self-associates to form a very stable tetramer. This tetramerization region is sufficient for complex formation with Ssn6 (20) and binds to the first three TPR motifs of Ssn6, which comprise the minimal domain necessary for binding to Tup1 and for mediating repression of cell type-specific genes (11, 30). We have quantitated the affinity of the binding of Tup1 to Ssn6 and found that the equilibrium dissociation constant is in the 100 nM range. Substitution of an arginine in place of leucine 62 in the Tup1 protein decreases this affinity of binding to Ssn6 by 100-fold. Because this mutation has little effect on either the secondary structure of the Tup1 N-terminal domain or on its ability to tetramerize, these data suggest that residue 62 is likely to lie on the surface of the Tup1 tetramer and participate in direct interactions with the Ssn6 protein.

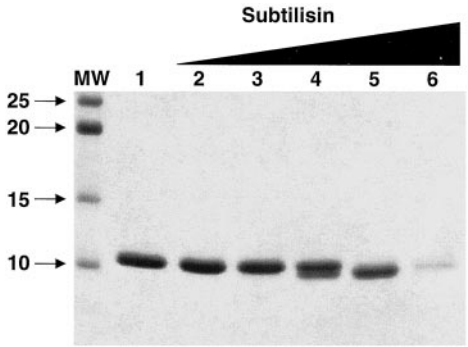

FIG. 5. **Limited proteolysis of Sc N91 Tup1.** SDS-polyacrylamide gel electrophoresis gel showing digestion of Sc N91 Tup1 with increasing concentrations of subtilisin. Positions of molecular weight markers are shown on the *left*. Increasing subtilisin concentration is denoted by the wedge above the gel. Digest mixtures contained 4 μg/ml Sc N91 Tup1 in 100 mM ammonium bicarbonate with 0 μg/ml (*lane 1*), 0.02 μg/ml (*lane 2*), 0.1 μg/ml (*lane 3*), 0.2 μg/ml (*lane 4*), 1 μg/ml (*lane 5*), or 2 μg/ml subtilisin (*lane 6*). Digests were incubated at 24 °C for 30 min, stopped with the SDS loading buffer, and boiled for 3 min before loading.

The results from CD spectroscopy, analytical ultracentrifugation, x-ray diffraction, ^{1}H NMR, and protease digestion experiments suggest that the Tup1 N-terminal domain is an extended helix that self-associates to form a 4-helix bundle. The model of the Tup1 N-terminal domain as an extended α-helix reconciles the initial apparent contradiction between the high α-helical content indicated by the CD spectrum and the absence of peak dispersion in the amide and methyl group resonance ranges in the ^{1}H nuclear Overhauser effect spectroscopy NMR spectrum. This might be expected to give rise to a lack of dispersion in the proton NMR spectrum because of a lack of tertiary folding of the protein monomer, resulting in a uniform environment for amide and methyl group protons. Because this domain of Tup1 is protease-resistant and forms a monodisperse solution of tetramers, it is highly unlikely that the lack of dispersion in the spectrum results from a global unfolding of the protein. The model for the structure of the tetramerization domain of Tup1 is strongly supported by x-ray diffraction data from disordered crystals of the N-terminal domain of Tup1 showing the presence of a fiber diffraction characteristic of coiled-coil proteins. This result is consistent with an analysis of the Tup1 N-terminal sequences with programs predicting coiled coils (MultiCoil (43) and Coiled Coil Prediction (44)), which show that this region has a high propensity to form coiled coils (data not shown).

The present data are consistent with several possible arrangements of helices in the Tup1 N-terminal domain tetramer. The simplest model for the tetramer is a 4-helix bundle composed of four α-helices, each about 24 turns in length, organized in either a parallel or alternating antiparallel fashion. Such an arrangement would give rise to a tetramer of

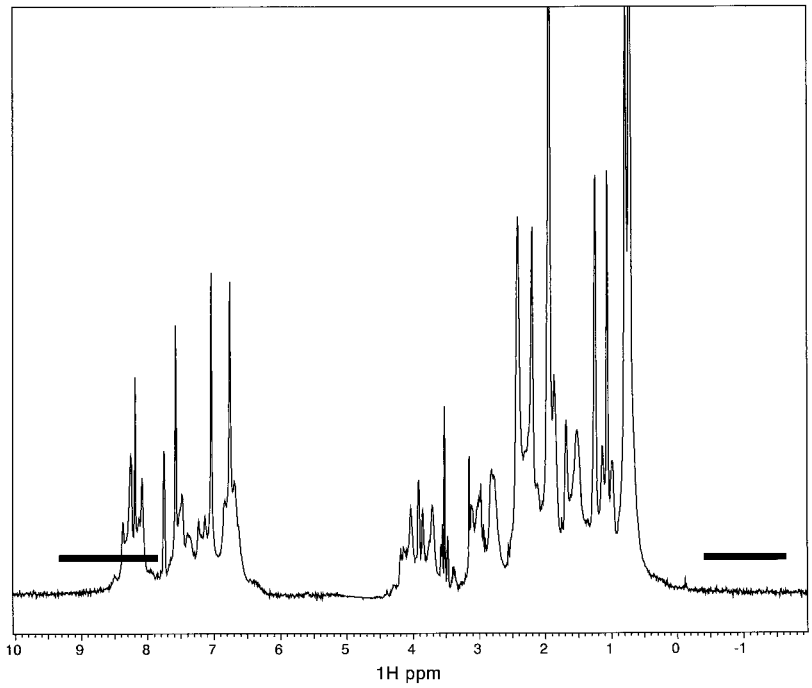

FIG. 6. **NMR spectrum of Sc N91 Tup1.** 1H nuclear Overhauser effect spectroscopy spectrum of Sc N91 Tup1 in 20 mM phosphate buffer (pH 7) is shown. *Thick black lines* show the absence of peak dispersion in the amide and methyl group resonance ranges.

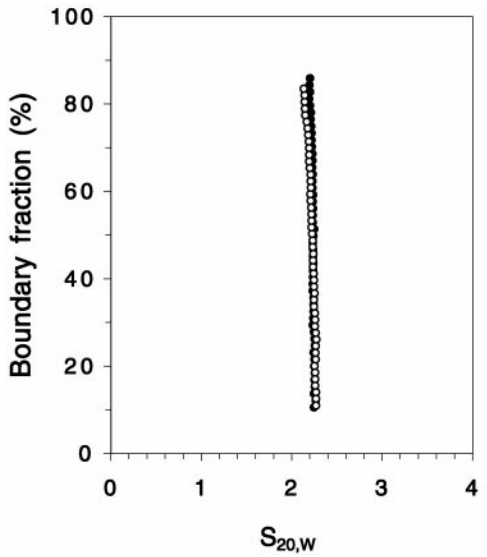

FIG. 7. **Integral distribution of sedimentation coefficients for ScN91 Tup1.** Boundary fraction *versus* $S_{20,w}$ for 0.18 mg/ml (●) and 1.1 mg/ml (○) of Sc N91 Tup1.

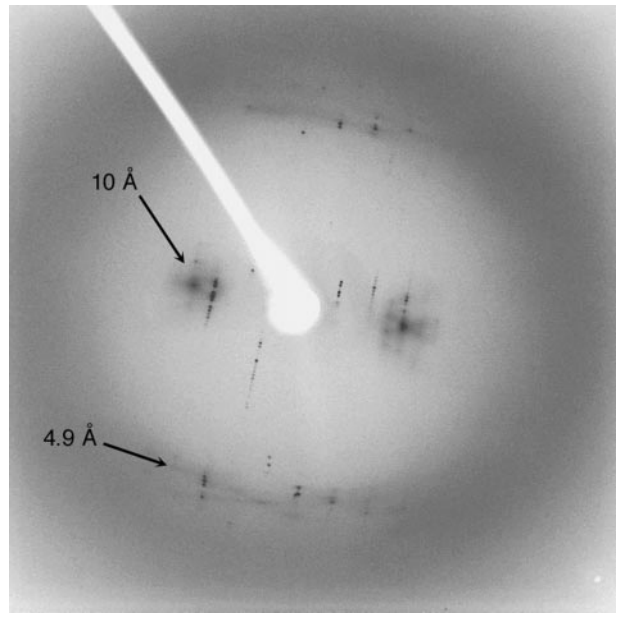

FIG. 8. **Diffraction from crystals of N91 Tup1 showing characteristic coiled-coil fiber pattern.** The meridional streaks and strong reflections in the 4.9 Å region are the result of the vertical rise/subunit in the helices, which are oriented approximately along the vertical axis. The 10 Å diffraction spots in the perpendicular result from the side to side packing of the helices in the coiled coil, which are separated by an average spacing of 10 Å.

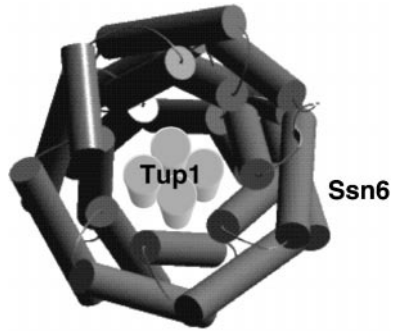

FIG. 9. **Model of the Tup1·Ssn6 complex.** The model of the 10 TPR repeats of Ssn6 was built using the coordinates of a multiple TPR motif protein constructed by D. Barford (30) based on the tandem TPR repeats of PP5 (Protein Data Bank code 1A17 (31)). The four cylinders drawn along the axis of the superhelical 10 TPR model are an artificial representation of the 4-helix bundle model of the N-terminal domain of Tup1. This diagram was produced using SETOR (53).

approximately 125 Å in length and 25 Å in diameter, consistent with velocity sedimentation results showing the tetramer to be highly asymmetric in shape. The meridional streaks at 4.9 Å resolution in the fiber diffraction data indicate that the helix-crossing angles in the Tup1 tetramer are likely to be larger than those in classical two-stranded coiled coils, which give rise to meridional reflections at 5.1 Å resolution (41, 42, 45). It is also possible that only part of each N-terminal domain monomer participates in an alternating antiparallel 4-helix bundle tetramer interface. In this quaternary arrangement, the N-terminal portion of each helix would form an antiparallel 4-helix bundle, with the two C termini that project from each end of the core tetramerization domain coiling around one another to form two-stranded coiled-coil extensions. The latter arrangement could account for the high predicted axial ratio of the tetramer and is consistent with data showing that deletion of the 51 N-terminal amino acids disrupts tetramerization of the intact Tup1 protein (12).

The Tup1 tetramerization domain may share some structural similarity with the tetramerization domain of Groucho, a transcriptional repressor from *Drosophila melanogaster* that contains a WD40 domain similar in sequence character to that of Tup1 (46, 47). The tetramerization of the Groucho protein is dependent upon two putative amphipathic α-helices with a leucine-zipper motif, termed the LZL motif (48), at the N terminus of the protein. Although Tup1 lacks the LZL motifs, it shares with Groucho the presence of a helical N-terminal domain that mediates tetramerization. Although the sequence similarity between the two proteins' tetramerization domains falls below the level of significance (~18% identity with gaps in the alignment), it is quite possible that the two share a similar structure.

As mentioned above, the N-terminal domain of Tup1 mediates binding with the TPR domain of Ssn6. The crystal structure of the TPR domain of the protein phosphatase 5 showed that the arrangement of the α-helices of multiple TPR repeats generates a right-handed superhelix with an amphipathic groove on the inner face of the superhelix (31). TPR repeats bear some resemblance to the repeating motifs in other superhelical proteins. One example is the armadillo repeat, which is found in proteins such as the *Drosophila* protein Armadillo, the cytoskeletal protein β-catenin, and the tumor suppressor gene product Adenomatous Polyposis Coli (49). The crystal structure of β-catenin revealed that the armadillo domain also consists of a right-handed superhelix of α-helices possessing a long positively charged groove predicted to be the site of protein-protein interactions (50). Importin β and the protein phosphatase 2A PR65/A are other examples of all helical proteins containing 19 and 15 HEAT repeats, respectively. Similar to a TPR repeat, the HEAT repeat is composed of two helices connected by a short turn (51). The helices of the HEAT domain of the protein phosphatase 2A PR65/A generate a left hand superhelical conformation (52), whereas the helices of the HEAT domain of importin-β are arranged in a right-handed superhelix (51). The HEAT domain of importin-β binds to a 43-residue region of importin-α termed the importin-β binding domain, which contains a N-terminal extended moiety and a C-terminal α-helix. In the crystal structure of the complex formed by these two proteins (51), the HEAT repeats of importin-β form a superhelical structure that wraps around the importin-β binding domain helix. A comparison of two independent structures of importin-β (51) indicates that HEAT repeat domain of impor-

tin-β is flexible, thereby permitting conformational changes that allow the tandem HEAT repeats of importin-β to wrap around the helical importin-β binding domain of importin-α (51).

The structure of the complex formed by the HEAT repeat protein importin-β with the helical importin-α protein suggests a possible model for how the TPR repeats of Ssn6 may complex with the helical tetramerization domain of Tup1, giving rise to the 4:1 Tup1·Ssn6 complex. Ssn6 contains 10 TPR motifs which, as seen in PP5 (31), are also likely to form a superhelical structure with an inner groove. The proposed 4-helix bundle formed by the N-terminal domain of Tup1 could fit in the Ssn6 inner groove in a manner similar to the interaction observed between importin-β and the importin-β binding domain (Fig. 9). As proposed by Das *et al.* (31), a single α-helix could fit into the inner groove of the TPR repeats with no change in the superhelical pitch observed in the PP5 structure. It is possible that, as in the case of the importin-β, there is flexibility in the TPR domain of Ssn6 that would allow the repeats to wrap around the Tup1 4-helix bundle. Three TPR motifs are the minimum number of repeats necessary to form the internal groove (31), which could explain why three consecutive TPR repeats of Ssn6 are sufficient to interact with the N-terminal domain of the Tup1 protein. In our proposed model, the outer surface of the Ssn6 TPR domain is available for interactions with other transcription factors, like the DNA binding factors that recruit the repressor complex Tup1·Ssn6. Because distinct combinations of TPR motifs are required for repression of distinct classes of genes (11), each DNA binding factor likely interacts with a particular set using the outer surface, which would be different for each DNA binding factor. Confirmation of this model awaits a detailed structural analysis of the Tup1·Ssn6 complex.

Acknowledgments—We thank C. Garvie for discussions; N. Laronde-Leblanc for providing the AraC protein; A. D. Johnson for plasmids; R. Gitti and M. Summers (Howard Hughes Medical Institute, UMBC, Baltimore) for NMR data collection and for discussion; D. Barford for sharing coordinates of PP5 as well as theoretical models of TPR proteins. SEDNTERP was developed by J. Philo, D. Hayes, and T. Laue; Ultrascan II was developed by B. Demeler.

REFERENCES

1. Mukai, Y., Harashima, S., and Oshima, Y. (1991) *Mol. Cell. Biol.* **11,** 3773–3779
2. Keleher, C. A., Redd, M. J., Schultz, J., Carlson, M., and Johnson, A. D. (1992) *Cell* **68,** 709–719
3. Schultz, J., and Carlson, M. (1987) *Mol. Cell. Biol.* **7,** 3637–3645
4. Trumbly, R. J. (1992) *Mol. Microbiol.* **6,** 15–21
5. Zitomer, R. S., and Lowry, C. V. (1992) *Microbiol. Rev.* **56,** 1–11
6. Elledge, S. J., Zhou, Z., Allen, J. B., and Navas, T. A. (1993) *Bioessays* **15,** 333–339
7. Nehlin, J. O., Carlberg, M., and Ronne, H. (1991) *EMBO J.* **10,** 3373–3377
8. Zhou, Z., and Elledge, S. J. (1992) *Genetics* **131,** 851–866
9. Balasubramanian, B., Lowry, C. V., and Zitomer, R. S. (1993) *Mol. Cell. Biol.* **13,** 6071–6078
10. Treitel, M. A., and Carlson, M. (1995) *Proc. Natl. Acad. Sci. U. S. A.* **92,** 3132–3136
11. Tzamarias, D., and Struhl, K. (1995) *Genes Dev.* **9,** 821–831
12. Varanasi, U. S., Klis, M., Mikesell, P. B., and Trumbly, R. J. (1996) *Mol. Cell. Biol.* **16,** 6707–6714
13. Redd, M. J., Arnaud, M. B., and Johnson, A. D. (1997) *J. Biol. Chem.* **272,** 11193–11197
14. Schultz, J., Marshall-Carlson, L., and Carlson, M. (1990) *Mol. Cell. Biol.* **10,** 4744–4756
15. Thrash-Bingham, C., and Fangman, W. L. (1989) *Mol. Cell. Biol.* **9,** 809–816
16. Trumbly, R. J. (1986) *J. Bacteriol.* **166,** 1123–1127
17. Carlson, M., Osmond, B. C., Neigeborn, L., and Botstein, D. (1984) *Genetics* **107,** 19–32
18. Flick, J. S., and Johnston, M. (1990) *Mol. Cell. Biol.* **10,** 4757–4769
19. Komachi, K., Redd, M. J., and Johnson, A. D. (1994) *Genes Dev.* **8,** 2857–2867
20. Tzamarias, D., and Struhl, K. (1994) *Nature* **369,** 758–761
21. Wahi, M., Komachi, K., and Johnson, A. D. (1998) *Cold Spring Harbor Symp. Quant. Biol.* **63,** 447–457
22. Kuchin, S., and Carlson, M. (1998) *Mol. Cell. Biol.* **18,** 1163–1171
23. Cooper, J. P., Roth, S. Y., and Simpson, R. T. (1994) *Genes Dev.* **8,** 1400–1410
24. Edmondson, D. G., Smith, M. M., and Roth, S. Y. (1996) *Genes Dev.* **10,** 1247–1259
25. Fong, H. K., Hurley, J. B., Hopkins, R. S., Miake-Lye, R., Johnson, M. S., Doolittle, R. F., and Simon, M. I. (1986) *Proc. Natl. Acad. Sci. U. S. A.* **83,** 2162–2166
26. Williams, F. E., and Trumbly, R. J. (1990) *Mol. Cell. Biol.* **10,** 6500–6511
27. Komachi, K., and Johnson, A. D. (1997) *Mol. Cell. Biol.* **17,** 6023–6028
28. Braun, B. R., and Johnson, A. D. (1997) *Science* **277,** 105–109
29. Goebl, M., and Yanagida, M. (1991) *Trends Biochem. Sci.* **16,** 173–177
30. Smith, R. L., Redd, M. J., and Johnson, A. D. (1995) *Genes Dev.* **9,** 2903–2910
31. Das, A. K., Cohen, P. W., and Barford, D. (1998) *EMBO J.* **17,** 1192–1199
32. Laue, T. M., Shah, B. D., Ridgeway, T. M., and Pelletier, S. M. (1992) in *Analytical Ultracentrifugation in Biochemistry and Polymer Science* (Harding, S. E., Rowe, A. J., and Horton, J. C., eds) pp. 90–125, Royal Society of Chemistry, London
33. Johnson, M. L., Correia, J. J., Yphantis, D. A., and Halvorson, H. R. (1981) *Biophys. J.* **36,** 575–588
34. van Holde, K. E., and Weischet, W. O. (1975) *Biopolymers* **17,** 1387–1403
35. Delage, G., and Geourjon, C. (1993) *Comp. Appl. Biosci.* **9,** 197–199
36. Andrade, M. A., Chacon, P., Merelo, J. J., and Moran, F. (1993) *Protein Eng.* **4,** 383–390
37. Bohm, G., Muhr, R., and Jaenicke, R. (1992) *Protein Eng.* **3,** 191–195
38. Delaglio, F. (1995) *J. Biomol. NMR* **6,** 277–293
39. Carrico, P. M., and Zitomer, R. S. (1998) *Genetics* **148,** 637–644
40. Tanford, C. (1961) *Physical Chemistry of Macromolecules*, pp. 358–359, John Wiley and Sons, Inc., New York
41. Rasmussen, R., Benvegnu, D., O'Shea, E. K., Kim, P. S., and Alber, T. (1991) *Proc. Natl. Acad. Sci. U. S. A.* **88,** 561–564
42. Crick, F. H. C. (1953) *Acta Crystallogr.* **6,** 689–697
43. Wolf, E., Kim, P. S., and Berger, B. (1997) *Protein Sci.* **6,** 1179–1189
44. Lupas, A., Dyke, M. V., and Stock, J. (1991) *Science* **252,** 1162–1164
45. Cohen, C., and Parry, D. A. (1990) *Proteins* **7,** 1–15
46. Parkhurst, S. M. (1998) *Trends Genet.* **14,** 130–132
47. Hartley, D. A., Preiss, A., and Artavanis-Tsakonas, S. (1988) *Cell* **55,** 785–795
48. Chen, G., Nguyen, P. H., and Courey, A. J. (1998) *Mol. Cell. Biol.* **18,** 7259–7268
49. Peifer, M., Berg, S., and Reynolds, A. B. (1994) *Cell* **76,** 789–791
50. Huber, A. H., Nelson, W. J., and Weis, W. I. (1997) *Cell* **90,** 871–882
51. Cingolani, G., Petosa, C., Weis, K., and Müller, C. W. (1999) *Nature* **399,** 221–229
52. Groves, M. R., Hanlon, N., Turowski, P., Hemmings, B. A., and Barford, D. (1999) *Cell* **96,** 99–110
53. Evans, S. V. (1993) *J. Mol. Graph.* **11,** 134–138
54. Collaborative Computational Project, November 4 (1994) *Acta Crystallogr. Sec. D* **50,** 760–763